

S.-W. Han,<sup>1,2</sup> C. H. Booth,<sup>1</sup> E. D. Bauer,<sup>3</sup> P. H. Huang,<sup>4</sup> Y. Y. Chen,<sup>4</sup> and J. M. Lawrence<sup>5</sup>
<sup>1</sup>*Chemical Sciences Division, Lawrence Berkeley National Laboratory, Berkeley, California 94720, USA*
<sup>2</sup>*Chonbuk National University, Jeonju, 561-756, Korea*
<sup>3</sup>*Los Alamos National Laboratory, Los Alamos, New Mexico 87545, USA*
<sup>4</sup>*Institute of Physics, Academia Sinica, Taipei, Taiwan, Republic of China*
<sup>5</sup>*Department of Physics, University of California, Irvine, California 92697, USA*

(Dated: March 23, 2006, Version 1.93)

When the particle size of  $\text{CeAl}_2$  and  $\text{CePt}_{2+x}$  samples is reduced to the nanometer scale, antiferromagnetism is suppressed and Kondo behavior dominates. We find that the Kondo temperature  $T_K$  can either decrease ( $\text{CeAl}_2$ ) or increase ( $\text{CePt}_{2+x}$ ) in the nanoparticles relative to the bulk. Extended x-ray absorption fine-structure data show that the Ce-Al and Ce-Pt environments are significantly distorted in the nanoparticles. While such distortions should strongly affect magnetic and electronic properties, we find they cannot explain the the observed changes in  $T_K$ . Changes in the conduction density of states or other parameters must, therefore, play a significant role.

PACS numbers: 72.15.Qm, 61.10.Ht, 71.23.-k, 61.46.+w

Despite the recent explosion in interest in fundamental processes at the nanoscale, comparatively few studies of the effect of decreasing particle size on strongly-correlated electron materials exist [1–3]. A recent exception involves the cerium-based Laves phase compounds:  $\text{CeAl}_2$ ,  $\text{CePt}_2$  and  $\text{CePt}_{2.5}$  display the fascinating property that as their particle size becomes comparable to the nanometer scale, they change from displaying Kondo behavior above an antiferromagnetic (AF) transition ( $T_N = 3.9$  K for  $\text{CeAl}_2$  [4] and 1.6 K for  $\text{CePt}_{2+x}$  [5, 6]) to displaying only a nonmagnetic, Kondo ground state [7, 8]. The suppression of the AF ground state in the nanoparticles is thought to be due to the inability of small particles to support spin waves [7], as related to spin fluctuations in these materials [4]. In addition, changes to the Kondo temperature  $T_K$  occur that are attributed at least partially to size effects [7]. However, an important component to the Kondo interaction is the  $f$ -electron/conduction electron hybridization, which is a local effect that depends strongly on the near-neighbor structural environment around the  $f$ -ions. Therefore, lattice distortions or disorder could play an equally important or even dominant role compared to particle size in determining interaction strengths and even whether or not the ground state is magnetic.

To clarify the structural issues, we report extended x-ray absorption fine structure (EXAFS) measurements on bulk and nanoparticle samples of  $\text{CeAl}_2$ ,  $\text{CePt}_2$  and  $\text{CePt}_{2.5}$  at the Ce and Pt  $L_{III}$  edges. These data indicate that large distortions exist in each of the nanophase materials. By using a tight-binding form for the hybridization matrix element  $V_{fc}$ , we demonstrate that, although these distortions are important, other size and surface-induced effects must also play a large role.

The nanoparticles are prepared by an evaporation method [7]. The average particle size is  $8.0 \pm 0.5$  nm in diameter for  $\text{CeAl}_2$  [7],  $3.8 \pm 0.3$  nm for  $\text{CePt}_2$  and  $4.2 \pm 0.3$

for  $\text{CePt}_{2.5}$ , as determined by high-resolution transmission electron microscopy. While the volume of  $\text{CeAl}_2$  expands by 1.1% relative to the bulk [7], the  $\text{CePt}_{2+x}$  nanoparticles *contract* by 6%. AF is observed in the bulk samples at 3.8 K, 1.6 K and 0.8 K, respectively. Estimates of  $T_K$  from the electronic coefficient  $\gamma = C_{el}/T$  to the linear part of the specific heat are hampered by the nearby AF ordering, but are estimated to be  $\sim 5$  K for  $\text{CeAl}_2$  [4] and 1 K for  $\text{CePt}_{2+x}$  [5]. The nanoparticles display no AF, but do display enhanced  $\gamma$ 's: The value

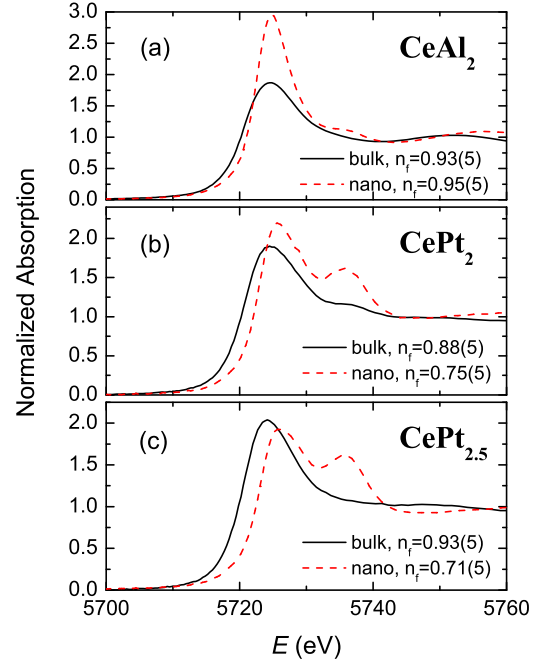


FIG. 1: Ce  $L_{III}$ -edge XANES at 20 K on (a)  $\text{CeAl}_2$ , (b)  $\text{CePt}_2$  and (c)  $\text{CePt}_{2.5}$ , together with estimates of  $n_f$ . Energy is calibrated by setting the first inflection point of the  $\text{CeO}_2$  Ce  $L_{III}$  edge to 5724.0 eV.

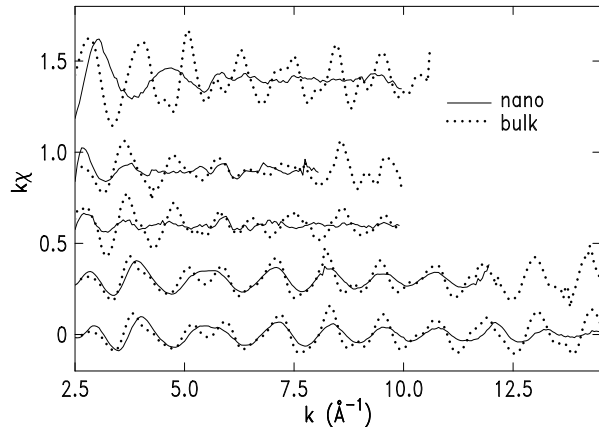


FIG. 2: EXAFS ( $k\chi$ ) as a function of  $k$  measured at 20 K. From top, Ce  $L_{III}$ -edge on  $CeAl_2$ ,  $CePt_2$  and  $CePt_{2.5}$ , and Pt  $L_{III}$ -edge on  $CePt_2$  and  $CePt_{2.5}$ . The Ce  $L_{III}$ -edge EXAFS data are limited to  $k = 10 \text{ \AA}^{-1}$  by the Ce  $L_{II}$ -edge.

$\gamma = 9 \text{ J mol}^{-1} \text{ K}^{-2}$  for nanoparticle  $CeAl_2$  is among the largest measured for any compound [7, 9].

The samples were reground for x-ray absorption measurements and passed through a  $20 \text{ }\mu\text{m}$  sieve. The sieved powder was spread uniformly over adhesive tape, cut into strips, and stacked to obtain samples with absorption edge steps corresponding to  $0.3 - 1.0$  absorption lengths. Transmission Ce and Pt  $L_{III}$ -edge x-ray absorption spectra on  $CeAl_2$  and  $CePt_{2.5}$  were obtained on BL 2-3 at the Stanford Synchrotron Radiation Laboratory (SSRL) using a half-tuned Si(111) double-crystal monochromator. Data were collected on  $CePt_2$  at the PNC-CAT of the Advanced Photon Source (APS) using a 3/4-tuned Si(111) double-crystal monochromator.

The Ce  $L_{III}$ -edge x-ray absorption near-edge structure (XANES) results are displayed in Fig. 1, after a pre-edge background subtraction. Rare-earth XANES measurements are widely used for determining valence of cerium compounds (for instance, see Ref. [3]). The data show a dramatic change between the bulk and nanoparticle samples, with the first main peak near 5725 eV noticeably sharper in the nanoparticle spectra. A new peak appears in the nanoparticle  $CePt_{2+x}$  spectra near 5735 eV, indicative of a shift in the mean valence toward tetravalence. These spectra have been fit with a combination of arctangents and pseudo-Voigts to extract the  $f$ -electron occupancy  $n_f$ . This procedure has been shown to be accurate within  $\sim 5\%$  [3]. These data show that Ce in  $CeAl_2$  remains close to trivalent, consistent with the high value of  $\gamma$  [7], while the strongly mixed-valent character of the  $CePt_{2+x}$  nanoparticle samples is known to correlate with large Kondo temperatures,  $T_K > 100 \text{ K}$  [10].

EXAFS data were analyzed with the UWXAFS package [11] using standard procedures [12] and photoelectron back-scattering functions calculated with the FEFF8 code [13]. After the atomic background absorption  $\mu_0$

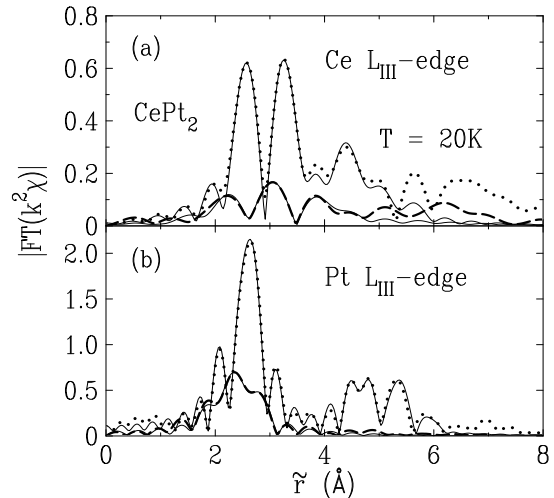


FIG. 3: FT magnitude of EXAFS data from bulk (dotted) and a nanoparticle (thick-dashed) samples of  $CePt_2$  from (a) the Ce edge and (b) the Pt edge. Solid lines are best fits. Ce edge data are transformed from  $2.7 - 7.5 \text{ \AA}^{-1}$  (nanoparticles) or  $2.5 - 9.5 \text{ \AA}^{-1}$  (bulk). Pt data are transformed from  $2.5 - 14.5 \text{ \AA}^{-1}$  (bulk) or  $2.5 - 11.5 \text{ \AA}^{-1}$  (nanoparticles). All FT's use a Hanning window of width  $0.5 \text{ \AA}^{-1}$ .

was determined, the EXAFS function  $\chi = \mu/\mu_0 - 1$  was obtained. Figure 2 shows the EXAFS for all three samples as a function of the photoelectron wave vector  $k = \hbar^{-1}\sqrt{2m_e(E - E_0)}$ , where  $m_e$  is the electron rest mass,  $E$  is the incident photon energy and  $E_0$  is the edge energy, chosen arbitrarily at the half-height of the edge. The weak EXAFS oscillations from the nanoparticles indicate that their local structures are considerably disordered compared to their bulk counterparts.

Figure 3 shows the magnitude of the Fourier transformed (FT) EXAFS data from bulk and nanocrystalline samples of  $CePt_2$ . FT data for  $CeAl_2$  [14] and  $CePt_{2.5}$  are similar to the  $CePt_2$  transforms. Note that peaks are shifted from their true pair distances due to the phase shift of the back scattered photoelectron. Detailed fits are therefore necessary to obtain quantitative information. Fits to the bulk data start from the  $C15$  Laves structure (space group  $F\bar{4}3m$ ), allowing the pair distances and the variance of the pair-distance distributions  $\sigma^2$  (which include thermal vibrations and static disorder) for each shell below  $7 \text{ \AA}$  to vary. The immediate environment around the Ce atoms on the  $4a$  and  $4c$  sites consists of 12 Al or Pt nearest neighbors arranged in an irregular octahedron, closely followed by 4 Al or Pt atoms. The local environment around the Al and Pt atoms consists of 6 nearest-neighbor Al or Pt's followed by 6 Ce's at a somewhat longer distance. Note that the  $CePt_{2.5}$  sample nominally has Pt on 1/7th of the  $4a$  and  $4c$  sites. The amplitude fractions for all pairs are held fixed to the nominal values in the fits to the bulk data. Fit quality for bulk samples is high, and the number of fit param-

TABLE I: Fit results at 20 K. A single value of  $S_0^2$  and  $\Delta E_0$  was used for each sample at each edge.  $S_0^2$  was determined from the bulk sample by fixing the number of neighbors  $N$  to the nominal values, and then used for the nanoparticle data.

	pair	$S_0^2$	$N$	Bulk Sample		Nanoparticle Sample		
				$r(\text{\AA})$	$\sigma^2(\text{\AA}^2)$	$N$	$r(\text{\AA})$	$\sigma^2(\text{\AA}^2)$
CeAl <sub>2</sub>	Ce-Al	0.90(6)	12	3.356(5)	0.0038(4)	11(2)	2.96(2)	0.044(9)
	Ce-Ce		4	3.503(6)	0.0021(7)			
	Ce-O							
CePt <sub>2</sub>	Ce-Pt	0.85(10)	12	3.18(1)	0.012(1)	11(1)	2.91(1)	0.025(7)
	Ce-Ce		4	3.43(1)	0.002(1)	3.8(6)	3.37(1)	0.017(5)
	Ce-O					1.5(6)	2.50(5)	0.025(9)
	Pt-Pt	0.83(5)	6	2.723(2)	0.0015(2)	6.4(5)	2.690(5)	0.0051(2)
	Pt-Ce		6	3.19(1)	0.013(1)	6(1)	2.86(2)	0.048(8)
CePt <sub>2.5</sub>	Ce-Pt	0.95(10)	12	3.18(1)	0.014(1)	10.8(10)	2.84(1)	0.021(1)
	Ce-Ce/Pt <sup>a</sup>		4	3.44(2)	0.003(1)	3.9(5)	3.29(1)	0.024(2)
	Ce-O					1.6(3)	2.39(3)	0.020(6)
	Pt-Pt	0.85(7)	5.6	2.713(2)	0.0019(2)	6.1(6)	2.690(3)	0.0056(3)
	Pt-Ce/Pt <sup>a</sup>		5.87	3.13(1)	0.014(1)	5.5(9)	2.92(3)	0.034(5)

<sup>a</sup>6/7th of  $N$  are Ce, 1/7th are Pt,  $R$  constrained to the same value,  $\sigma^2$ 's constrained by the ratio of the reduced masses.

ters is well below the number of degrees of freedom, as estimated by Stern's rule [15]. The fit results are summarized in Table I. The small measured  $\sigma^2$ 's for bulk CeAl<sub>2</sub> (eg. Ce-Al  $\sigma^2 = 0.0038 \text{ \AA}^2$ ) indicate that it is locally well ordered. The bulk  $\sigma^2$ 's for the CePt<sub>2+x</sub> samples indicate some disorder exists even in the starting material (eg. Ce-Pt in CePt<sub>2</sub>  $\sigma^2 = 0.012 \text{ \AA}^2$ ). In any case, the measured local pair distances agree well with the average structures derived from diffraction measurements [5, 16].

The fit results to the nanoparticle data are more complex. Reliable results are not obtained for the Ce-Ce or more distant shells in CeAl<sub>2</sub> nanoparticles. CeO<sub>2</sub> contamination is expected [7], and in fact the fit is considerably improved by including  $1.2 \pm 0.6$  oxygens at  $\sim 2.44 \text{ \AA}$ , along with the main Ce-Al pairs at  $2.96 \text{ \AA}$ . The Ce-O amplitude is consistent with  $\sim 15\%$  CeO<sub>2</sub>, in agreement with Ref. [7], although the bond length is somewhat larger than the bulk CeO<sub>2</sub> value of  $2.34 \text{ \AA}$  [17]. The situation is similar for the CePt<sub>2+x</sub> nanoparticles. The fits are not sensitive to Pt-O contamination or Ce-O in further shells within  $\sim 20\%$ , nor are they sensitive to Ce/Pt site interchange beyond the nominal concentrations within  $\sim 12\%$ .

In any case, the average  $\sigma^2$  of the Ce-Al and Ce-Pt pairs is much larger and their pair distances are considerably shorter than that of the same pairs in the bulk samples. Ce-Ce pairs in the CePt<sub>2+x</sub> samples show a somewhat smaller contraction than the Ce-Pt pairs, but also show a large amount of disorder in the nanoparticles. Note that the same Ce-Pt pair distance is measured from the Pt  $L_{III}$  edge. Also note that the number of neighbors in the nanoparticles is similar to the bulk value, although the error bars are large beyond the nearest-neighbors.

While these measurements indicate that both large distortions and intrinsic disorder exist around Ce in the nanoparticles, the local structure is still describable as a Laves phase. Interestingly, the Pt-Pt pairs, which are

about the same distance as in elemental Pt [17], contract only slightly compared to those in the bulk CePt<sub>2+x</sub> samples. This contraction is nearly equal to that expected from the change in the cell volume, so we assume that the Pt's (and by analogy, the Al's) determine the lattice constant. This rigidity indicates that the Pt octahedrons remain approximately the same size in the nanoparticles. Since the Ce-Pt pairs have strongly contracted, the Ce atoms must not be at the center of the Pt octahedrons. A similar argument holds for the CeAl<sub>2</sub> nanoparticles. In this case, the measured pair distance would be dominated by the shortest atom pairs and a large static component to  $\sigma^2$  would develop, consistent with the observations. An analysis [18] to search for a skewed pair-distance distribution was, however, inconclusive.

Although the microscopic nature of the distortions remains unclear, further details can be inferred. For instance, it is possible that Ce distorts everywhere within a given nanoparticle in the same way. However, a more likely scenario is that some surface reconstruction occurs with Ce migrating toward the surface. Any oxide layer would have the same effect. If such a migration takes place, a distribution of distortions within a single nanoparticle will develop. One then expects different distortions corresponding to different particle sizes. All of these scenarios should occur at some level, and will have important consequences for the magnetic interactions.

Although modeling all these effects would ideally use a real many-body calculation, much can be learned by considering the Kondo interactions in the simple form  $T_K = W \exp[-\epsilon_f/(\rho V_{fc}^2)]$ . Both the conduction bandwidth  $W$  and the density of states at the Fermi level  $\rho$  depend on long-range effects and are difficult to predict in the nanophase.  $V_{fc}$ , however, is dominated by local interactions, so a tight-binding model [19] can be employed. The  $f$ -level energy  $\epsilon_f$  should not change much between

the bulk and nanophase material. Using this model, we assign to  $V_{fc}$  changes in  $T_K$  that are due only to the structural distortions. Particle size effects are then described by changes in  $W$  and  $\rho$ . We can then test whether particle-size effects are important in these materials by fixing  $W$  and  $\rho/\epsilon_f$  based on the measurement of  $T_K$  in the bulk sample, and then comparing the expected change in  $T_K$  due to changes in  $V_{fc}$  to the measured nanoparticle  $T_K$ 's. The relevant tight-binding form for  $V_{fc}$  is

$$V_{ll'} = \sum_{\text{pairs}} \frac{\eta_{ll'} \hbar^2}{m_e} \frac{\sqrt{r_l^{2l+1} r_{l'}^{2l'+1}}}{R_{ll'}^{l+l'+1}}, \quad (1)$$

where  $l$  and  $l'$  are the angular momentum quantum numbers of the  $f$  and the conducting electronic shells,  $r_l$ 's are the effective shell radii (tabulated in Ref. [19]), and  $R_{ll'}^{l+l'+1}$  is the distance between the  $l$ -ion and the  $l'$ -ion. The constant  $\eta_{ll'}$  is (assuming  $\sigma$  bonds)  $\eta_{fp} = 14.6$  and  $\eta_{fd} = 141.2$  for the cases given here [19].

Ignoring changes in sign and using these equations with the bulk  $\text{CeAl}_2$  crystal structure,  $V_{fp}(\text{bulk}) = 1.81$  eV. If we assume  $W = 1$  eV and  $T_K = 5$  K, then  $\epsilon_f/\rho = 25.4$  eV<sup>2</sup>. Using the lattice constants for the nanoparticle, but assuming no other distortions, gives  $V_{fp}(\text{nano}) = 1.78$  eV, and with the above values of  $W$  and  $\epsilon_f/\rho$ ,  $T_K = 3.8$  K. As noted by Chen *et al.* [7] using a different scaling argument, this value is still  $\sim 5$  times larger than the observed value, and they ascribe the difference to surface or size effects. These effects would presumably be manifest as a decrease in either  $\rho$  and/or  $W$  in the nanoparticle, either of which seem likely. This analysis is not qualitatively affected by assuming a very different  $W$ .

Disorder is known to give a distribution of Kondo temperatures [20], and hence the local structure distortions reported here should be included when evaluating Eq. 1. Evaluating this sum shows that distortions consistent with our measurement, of order  $0.03$ - $0.04$  Å<sup>2</sup>, give on average an even larger hybridization than in the ordered bulk sample, implying a higher, not lower,  $T_K$ . This analysis places most of the burden for decreasing  $T_K$  on the longer-range, size-induced effects of  $W$  and  $\rho$ .

The situation is reversed for the  $\text{CePt}_{2+x}$  samples, since  $T_K$  is observed to increase in the nanoparticle (on the order of 100 K) relative to the bulk material ( $T_K \approx 1$  K). Using a similar procedure as above and the measured lattice constants for both bulk and nanoparticle  $\text{CePt}_2$  samples,  $V_{fd}$  should increase from 1.86 eV in the bulk to 2.11 eV in the nanoparticle, corresponding to a  $T_K$  of 8 K. Including the measured distortions nearly doubles this estimate of  $T_K$ , which is not enough to explain the observed strong mixed valence in Fig. 1. A dramatic increase in  $\rho$  or  $W$  is likely necessary, such has been observed in vanadium nanoparticles [21].

In summary, we have studied the local electronic and structural properties of nanocrystalline  $\text{CeAl}_2$ ,  $\text{CePt}_2$  and  $\text{CePt}_{2.5}$ . While cerium in  $\text{CeAl}_2$  remains close to

trivalent in the nanoparticle, a strong shift toward mixed valence occurs in the  $\text{CePt}_{2+x}$  nanoparticles. In addition, a substantial off-center distortion of the Ce atoms in the nanoparticles is observed. Despite the magnitude of this distortion, we find that it cannot explain either the sign or the magnitude of the observed changes in the electronic specific heat, demonstrating that long-range effects such as the conduction bandwidth and the density of states at the Fermi level are in direct competition with the structural distortions. These effects create a complicated landscape for exploring Kondo interactions under the influence of size and disorder effects.

This work was supported by the Office of Science, U.S. Department of Energy (DOE) under Contract No. DE-AC02-05CH11231. Data were collected at the SSRL and at the APS, both national user facilities supported by the US DOE and Office of Basic Energy Sciences.

- 
- [1] W. B. Thimm, J. Kroha, and J. von Delft, *Phys. Rev. Lett.* **82**, 2143 (1999).
  - [2] P. Schlottmann, *Phys. Rev. B* **65**, 024431 (2002).
  - [3] C. H. Booth *et al.*, *Phys. Rev. Lett.* **95**, 267202 (2005).
  - [4] F. Steglich, C. D. Bredl, M. Loewenhaupt and K. D. Schotte, *J. Phys. (Paris) Colloq.* **40**, C5-301 (1979), and references therein.
  - [5] J. M. Lawrence *et al.*, *Phys. Rev. B* **56**, 5 (1997).
  - [6] R. R. Joseph, K. A. Gschneidner, Jr. and R. E. Huggsgerg, *Phys. Rev. B* **5**, 1878 (1972); L. Rebelsky, K. Reilly, S. Horn, H. Borges, J. D. Thompson and R. Caspary, *J. Appl. Phys.* **67**, 5206 (1990); A. B. Andrews, J. J. Joyce, A. J. Arko, J. D. Thompson, J. Tang, J. M. Lawrence and J. C. Hemminger, *Phys. Rev. B* **51**, R3277 (1995).
  - [7] Y. Y. Chen *et al.*, *Phys. Rev. Lett.* **84**, 4990 (2000).
  - [8] Y. Y. Chen *et al.* (unpublished).
  - [9] Heat capacity and susceptibility measurements of  $\text{CePt}_{2+x}$  indicate not all cerium atoms participate in the magnetic interactions, making an estimate of  $\gamma$  more difficult. This result will be the subject of a future paper.
  - [10] N. E. Bickers, D. L. Cox, and J. W. Wilkins, *Phys. Rev. B* **36**, 2036 (1987).
  - [11] E. A. Stern *et al.*, *Physica B* **208 & 209**, 117 (1995), see also <http://depts.washington.edu/uwxafs>.
  - [12] S.-W. Han *et al.*, *Phys. Rev. B* **66**, 094101 (2002).
  - [13] A. L. Ankudinov *et al.*, *Phys. Rev. B* **58**, 7565 (1998).
  - [14] S.-W. Han *et al.*, *J. Magn. Magn. Mater.* **272-276**, E101 (2004).
  - [15] E. A. Stern, *Phys. Rev. B* **48**, 9825 (1993).
  - [16] W. H. Zachariasen, *Acta. Cryst.* **2**, 388 (1949).
  - [17] R. W. G. Wyckoff, *Crystal Structures*, 2nd ed. (Interscience Publishers, New York, 1964).
  - [18] P. Eisenberger and G. S. Brown, *Solid State Commun.* **29**, 418 (1979).
  - [19] W. A. Harrison, in *Elementary Electronic Structure* (World Scientific, London, 1999), p. 644.
  - [20] C. H. Booth *et al.*, *Phys. Rev. B* **65**, 245114 (2002).
  - [21] O. Vergara, D. Heitkamp, and H. v. Löhneysen, *J. Phys. Chem. Solids* **45**, 251 (1984).